Surfaces and Interfaces 25 (2021) 101205

Contents lists available at ScienceDirect

Surfaces and Interfaces

journal homepage: www.sciencedirect.com/journal/surfaces-and-interfaces

LIPSS manufacturing with regularity control through laser wavefront curvature

A. San-Blas [a,b,*], M. Martinez-Calderon [a,b,#], E. Granados [c], M. Gómez-Aranzadi [a,b], A. Rodríguez [a,b], S.M. Olaizola [a,b]

[a] Ceit-Basque Research and Technology Alliance (BRTA), Manuel Lardizabal 15, 20018 Donostia/San Sebastián, Spain
[b] Universidad de Navarra, Tecnun, Manuel Lardizabal 13, 20018 Donostia/San Sebastián, Spain
[c] CERN, 1217 Geneva, Switzerland

ARTICLE INFO

Keywords:
LIPSS
Laser
Femtosecond
Nanostructure
Coherence
Regularity
Wavefront

ABSTRACT

Laser-Induced Periodic Surface Structures (LIPSS) manufacturing is a convenient laser direct-writing technique for the fabrication of nanostructures with adaptable characteristics on the surface of virtually any material. In this paper, we study the influence of 1D laser wavefront curvature on nanoripples spatial regularity, by irradiating stainless steel with a line-focused ultrafast laser beam emitting 120 fs pulses at a wavelength of 800 nm and with 1 kHz repetition rate. We find high correlation between the spatial regularity of the fabricated nanostructures and the wavefront characteristics of the laser beam, with higher regularity being found with quasi-plane-wave illumination. Our results provide insight regarding the control of LIPSS regularity, which is essential for industrial applications involving the LIPSS generation technique.

1. Introduction

LIPSS are regular and periodic nanopatterns with periods ranging from tens to hundreds of nanometers. Their fabrication is highly versatile, since they can be fabricated with most types of pulsed lasers and in almost any material, ranging from dielectrics to metals. They also exhibit a high degree of geometrical freedom: period, height and orientation can be controlled through parameters such as the number of applied pulses and fluence [1], angle of incidence [2] polarization [3] or laser wavelength [4]. Although many types of LIPSS have been described, the most commonly discussed types are Low Spatial Frequency LIPSS (LSFL), with periods Λ similar to the wavelength of the laser λ ($\Lambda \sim \lambda$), and High Spatial Frequency LIPSS (HSFL), with periods much shorter than the laser wavelength ($\Lambda << \lambda$) [5]. Bonse et al. [6] recently discussed the two main existing theories about LIPSS formation: generation due to electromagnetic scattering and interference effects [7, 8], or as a consequence of hydrodynamic matter redistribution and diffusion effect [9]. The authors concluded that depending on the material and irradiation conditions, experimental observations showed signs supporting one or other (or both) theoretical approaches. Therefore, both of them remain valid within certain parameter range. This theoretical background can be used in novel experimental techniques and strategies that further improve the results obtained in LIPSS nanostructuring applications (e.g., through high reliability, ease of implementation in industry).

Nowadays, LIPSS nanostructuring is being extensively used as a method capable of generating periodic nanostructures smaller than the diffraction limit in a simple and effective procedure, consisting of a single-pass laser beam. It has proven its effectiveness in key applications such as the fabrication of geometrical phase elements [10], gas sensing [11], improved tribological properties towards drag reduction [12], cell migration control [13] or structural colorization [14].

Developments in laser technology and beam-focusing strategies have vastly increased the processing rates of LIPSS, currently meeting industry productivity demands. Namely, the use of lasers with high repetition rates in combination with galvanometer scanners [15] or lasers with high pulse energy with cylindrical lenses [16–18] has increased productivity by several orders or magnitude. However, applications still find their main limitation in the lack of control over the reproducibility and spatial regularity of nanostructures. To address these challenges, advances in the knowledge about the LIPSS formation phenomenon and the role of different irradiation parameters become

* Corresponding author.
E-mail addresses: asanblasg@gmail.com, asanblas@ceit.es (A. San-Blas).
Present address: The University of Auckland, Auckland 1142, New Zealand.

https://doi.org/10.1016/j.surfin.2021.101205
Received 25 January 2021; Received in revised form 16 March 2021; Accepted 13 May 2021
Available online 23 May 2021

critical. In this context, it is decidedly important to consider the achieved regularity in the processing of LIPSS, since the coherence in spatial distribution and period will determine their effectiveness in applications, such as those involving induced birefringence [19] or controlled reflectance and refraction [20]. However, there is not much literature available about the influence of processing parameters on LIPSS regularity, in particular when generated with beam shaping techniques, which hinders the research on LIPSS applications.

LIPSS present some degree of sinuosity that depends on the processing conditions and material employed, which is usually described as spatial coherence or regularity. When assessing LIPSS regularity, the Dispersion of LIPSS Orientation Angle (DLOA [21]) parameter proves useful. This parameter measures the weighted distribution of the orientations described by the sinuous shapes of the ripples over a large area. This results in a quantitative measurement of LIPSS spatial coherence that can be used to evaluate their regularity. Due to a lack of a better definition for LIPSS regularity or coherence, DLOA is generally used in the literature as an indicative of this property, with lower values of DLOA hinting at better coherence. DLOA has been correlated in previous works with material plasmonic properties and laser irradiation wavelength for single beam scanning [21].

In this work, we address the problem of reliably manufacturing LIPSS with controllable regularity, by studying the influence of 1D wavefront curvature of a cylindrically focused Gaussian beam in their generation. The introduction of a cylindrical lens allows us to observe the variations in wavefront curvature around the beam focus in a one-dimensional axis, without undesired effects from the radial symmetry that would arise from a spherical focusing. We were able to correlate the DLOA of the fabricated LIPSS nanopatterns with the laser wavefront curvature. This result indicates that LIPSS regularity can be controlled and even optimized with the laser beam wavefront, which, in the case of a Gaussian beam, is easily controllable by adjusting the position of the surface with respect to the focal plane. We believe that this work provides good experimental ground for a better understanding of LIPSS formation while it can also help boosting their applications by providing a useful tool for efficient LIPSS manufacturing.

2. Experimental setup

A Ti:Sapphire laser beam was focused along the Y-axis onto the surface of the sample through a cylindrical lens with a focal length of 100 mm as shown in Fig. 1. The laser system ($M^2 < 1.3$) produced 120 fs pulses with a central wavelength of $\lambda = 800$ nm and a repetition rate of 1 kHz. Pulse energy was adjusted with a variable attenuator formed by a half-wave plate and a polarizer. A motorized half-wave plate was used to set the polarization of the laser beam parallel to the translation axis. XZ motorized stages were used to move the sample along the X-axis and to control the position in the Z-axis.

To better understand how the sample position relative to the beam focus affects the processing, a complete characterization of the beam size around its focus (this is, the focus along the X-axis) was made with a calibrated CCD (Fig. 2), measuring the beam half-width at $1/e^2$ in both directions (w_x and w_y). The intensity profile of the focused beam showed a Gaussian distribution with high ellipticity due to the very different axes w_x and w_y (a constant value of $w_y = 6$ mm was found in the studied range). Since the elliptic beam can be considered as two independent beams in the X- and Y- axes [22], the values found for $w_x(z)$ were fitted to the propagation of a Gaussian beam along the X-axis (Fig. 2) according to the well-known equation $w_x(z) = w_{0x}\sqrt{1+\left(\frac{z-z_0}{z_{Rx}}\right)^2}$, where w_{0x} is the waist. z is the distance along the beam propagation axis, with $z_0 = z(w_{0x})$, and z_{Rx} is the Rayleigh length. The corresponding wavefront curvature radius for such a Gaussian beam in the x-axis, R_x, is described by [22] $R_x = (z - z_0)\left(1+\frac{z_{Rx}}{z-z_0}\right)^2$, with the wavefront curvature being its inverse, R_x^{-1}.

Therefore, a cylindrically focused beam generates a highly elliptical spot around the focal plane of the lens, whose wavefront along the non-focused axis remains approximately constant in the propagation around the focus of the lens, leaving the variation of wavefront curvature in the X-axis as the only variable in this matter. On the other hand, the wavefront generated near the focal plane of a beam focused with a spherical lens presents radial symmetry. This leads to a situation in linear scanning configurations where it would be difficult to decorrelate the influence on LIPSS formation of scanning direction and wavefront curvature.

The irradiated material was stainless steel (AISI 304). The raw samples were mechanically polished obtaining an average roughness of $R_a = 276.3$ Å. As a result, the surface of the sample presented lines with a clear directionality. Before and after the laser process the samples were

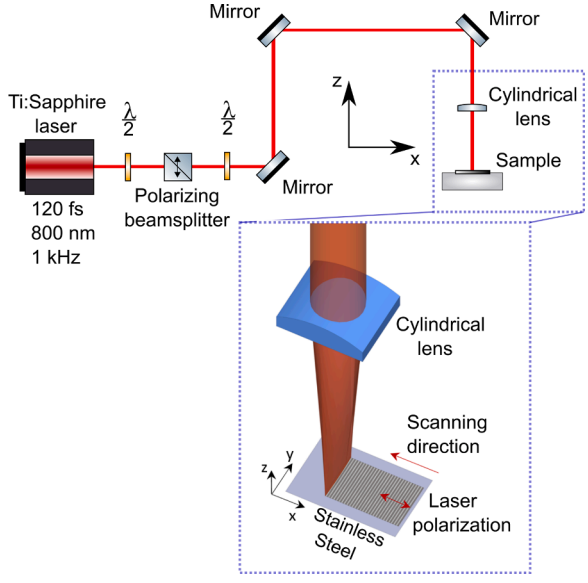

Fig. 1. Focusing system used in the processing of the samples. LSFL were produced perpendicular to the laser polarization. The sample was translated along the X-axis.

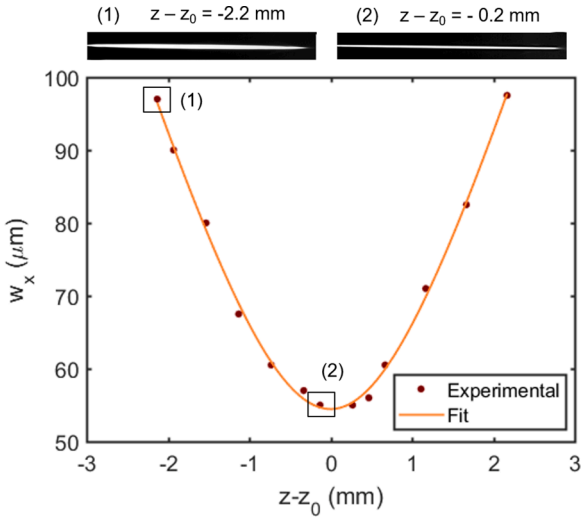

Fig. 2. Experimental values for w_x near the focus (maroon dots) and the corresponding fit to the propagation of a Gaussian beam (orange line). Optimal fit is found for values of w_{0x} = 54.5 μm and z_{Rx} = 1.46 mm. Inset: images of the focused beam at different focal planes (z-z_0 = -2.2 mm and -0.2 mm), with constant w_y = 6 mm, and w_x = 97 μm and 55 μm respectively.

introduced in an acetone ultrasonic bath for 3 min in order to remove dirt and particles generated during the process. Multiple samples were fabricated in a range of pulse energies E (0.55, 0.8, 1.4, 1.5, 1.75 and 2 mJ), processing speeds v (0.39, 0.625, 1, 1.6 and 2.56 mm/s) and distances z-z_0 (between -2 mm to +2 mm, every 0.2 mm) to provide different values for fluence and number of pulses. Average fluence per pulse F was calculated as $F = E/(\pi \bullet w_x \bullet w_y)$. The number of pulses N that overlap over a point in the sample during the non-static irradiation is $N = 2w_x/(v \bullet T)$, where T is the inter-pulse period of the laser [19].

The scanning direction was parallel to the directionality of the polishing lines. Polarization was also aligned with the scanning direction as seen in Fig. 3. This configuration between scanning direction, polishing lines and polarization gave the best results for LIPSS regularity. In this configuration, the polishing lines were erased in the writing of the LIPSS and showed no influence. However, when the polarization was perpendicular to the polishing lines (this is, with LIPSS parallel to the lines), the marks act as scattering sources generating LIPSS parallel to their orientation. Since the orientation of these lines is not perfectly consistent, this result in areas of LIPSS having slightly different orientations and showing discontinuities in the intersection among areas. Additionally, the relation between scanning direction and polarization was studied prior to the fabrication of the samples. The best regularities were observed for polarization parallel to the scanning direction (this is, with LSFL perpendicular to the advance of the laser beam), closely followed by perpendicular polarization. Regularity decreased for angles in between, with a clear minimum with diagonal polarization.

The surface of the processed steel was characterized with scanning electron microscopy (SEM). DLOA parameter was measured from these

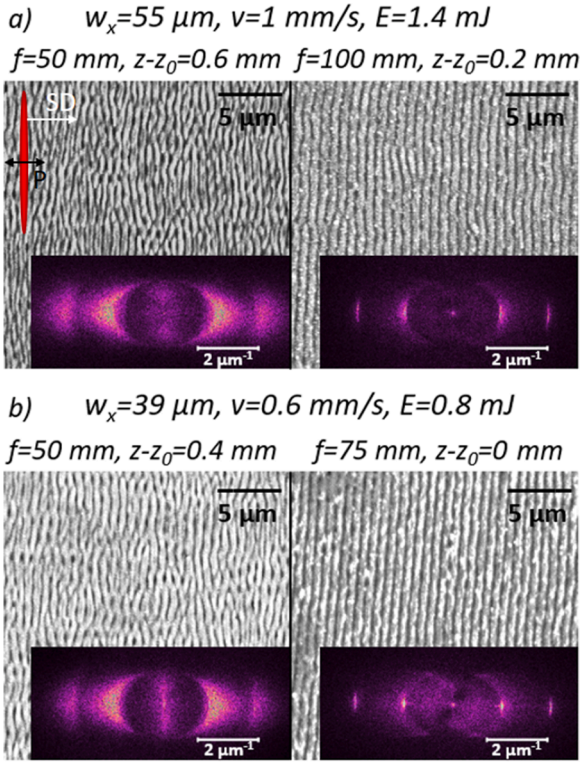

Fig. 3. Regularity comparison between pairs of samples with equal F and N and different distance to the focal plane. Examples (a) and (b) are provided in order to illustrate the behavior in a range of fabrication conditions. Processing parameters are shown in the image, resulting in: (a) $F = 0.14$ J/cm^2 and $N = 110$, (b) $F = 0.11$ J/cm^2 and $N = 130$. It can be seen that LIPSS are much more regular when the irradiation takes place near the focal plane, this is, when the wavefront shows less curvature, regardless of other parameters (namely, F and N). Top-left corner: schematization of the beam shape, scanning direction (SD) and polarization (P) used in the presented samples.

images. The standard procedure for the measurement of DLOA was carried as explained in [21], this is, using the Orientation Distribution module in OrientationJ plugin available for ImageJ software. Specific parameters used were local window of 1 pixel with Riesz filters. The software then analyzes the local orientation of ripples and integrates them over the area covered by the image, resulting in a distribution centered on the main direction of the LIPSS. The FWHM of this curve is the DLOA value.

From the two-dimensional Fast Fourier Transform (2D-FFT) of the micrographs, LIPSS period was extracted. Samples with high noise in the FFT (when the DC component is much more intense than the peaks corresponding to the frequency) due to a lack of LIPSS formation, or formation at its early stages, as well as samples that exhibited a dominant double frequency (also known as Type-2s [6]) were discarded. In particular, LIPSS with double-frequency would disrupt the homogeneity in the type of LIPSS in our study, since we only take into consideration LSFL (Low Spatial Frequency LIPSS) with $\Lambda \sim \lambda$ (type-s).

In order to stablish a direct comparison between samples fabricated under similar irradiation conditions, additional cylindrical lenses of focal lengths 50 mm and 75 mm have been used. Due to the different propagation of the laser beam under said lenses, similar w_x are found for different propagation distances and, accordingly, for different wavefront curvatures. Hence, samples with equal F and N but different wavefront curvature can be fabricated. Fig. 3 shows two pairs of samples showing that fluence or number of pulses are not the only irradiation parameters that affect LIPSS regularity. It can be seen that in both cases, LIPSS show higher regularity near the focal plane, which has lower wavefront curvature. This can be observed in the SEM micrograph, where LIPSS are straight and continuous in the images on the right. This regularity continues uninterrupted within the region of approximately constant fluence along the projected laser line unless they reach an imperfection in the material. This means that their length is in the order of a few millimeters in our case, which could be overcome easily with a wider laser beam and a better-polished surface. Additionally, regularity can be clearly seen in their FFT transform, where the dispersion in angles (vertical axis) and periods (horizontal axis) is much smaller in the samples fabricated near the focus.

3. Results and discussion

The period of nanopatterns in the samples was found to be between 500 nm and 650 nm. Period holds a decreasing trend with increasing number of pulses as reported in literature [23] when fluence is kept constant. After discarding invalid samples as described in the previous section, 77 samples with LSFL remained. The fabrication parameters for these samples included the entire range of energies, distances and speeds previously detailed, with the exception of $v = 0.39$ mm/s for which no samples presented the required LIPSS. Their DLOA values found are between 7.6° and 12.4°. Although DLOA values vary depending on the image magnification of the micrograph used [24], similar values for steel are found in the literature [21,24]. In this work, a constant magnification of 950x is used, covering a processed area of 126 × 126 µm^2.

In order to analyze the influence of the distance to the focal plane in LIPSS regularity, DLOA has been averaged over the multiple samples with different fabrication conditions (this is, different E and v, resulting in a wide combination of F and N) for each z-z_0 distance measured. The results show great symmetry around the focus (Fig. 4, left axis). A minimum can be observed along the points of lowest w_x, exhibiting a plateau from -0.4 mm to +0.4 mm, where said minimum is kept constant. At larger distances, DLOA rapidly grows until maxima found at -1.4 mm and 1.2 mm, after which it decreases again. These values have been compared to the absolute value of the wavefront curvature radius, $|R_x|^{-1}$ (Fig. 4, right axis). It shows a minimum $|R_x|^{-1}$ (planar wavefront) in the focus of the beam followed by a fast increase up to a maximum at z-$z_0 = z_{Rx}$. Using the values found for the beam propagation fit, this

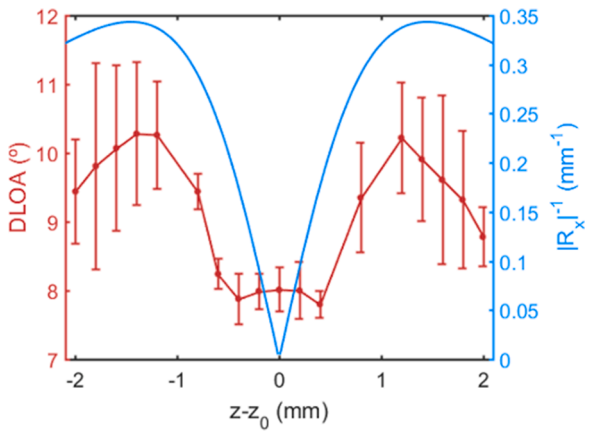

Fig. 4. Left axis (red): DLOA measured from the SEM micrographs at different distances along the propagation axis. Error bars are the standard deviation of the mean. Right axis (blue): absolute value of the wavefront curvature, $|R_x|^{-1}$, derived from the fit shown in Fig. 2. (For interpretation of the references to color in this figure legend, the reader is referred to the web version of this article.)

maximum is at $z_{Rx} = 1.46$ mm. Beyond this distance, the wavefront curvature slowly decreases with $|R_x|^{-1}$ $(\infty) \rightarrow 0$ mm^{-1}. Consequently, similar behavior can be observed between DLOA and $|R_x|^{-1}$, with a minimum in the focus for both parameters and maxima around z_{Rx}, continued by a decrease at larger distances.

This correlation between DLOA and wavefront curvature in a Gaussian beam has not been addressed in the theoretical or experimental literature to the best of our knowledge. The relation between the excitation of SPPs and LIPSS regularity has been studied in [21]. The influence of coherence in the laser source [25] and the effect of intrapulse interferences has been also studied [6,26]. These studies are in agreement with our results showing that a planar coherent wavefront generates LIPSS with higher regularity, which in the case of a Gaussian beam is related to DLOA as reported in Fig. 4. For other beam distributions, different relations could be found, such as the minimum DLOA being found outside the focal plane. This may be exploited with beam shaping or other techniques in order to extend the region of high regularity by maintaining low wavefront curvature through a larger propagation distance.

We believe that the main factor in the observed LIPSS behavior arise from the interference between surface plasmon polaritons (SPPs) generated at different defects within an area smaller than the propagation length (5 μm for the air/steel interface [21]). The lower curvature of the laser wavefront near the beam focus would lead to excitation of SPPs with similar conditions, coherently interfering with each other, resulting in LIPSS with high regularity.

Another factor that has been proposed to have an influence on regularity is the spot size [21]. According to this, a small irradiation spot increases the regularity of LIPSS since it reduces the interaction between SPPs generated from different defects. In general, this effect is better described by the SPP active area [27]. This parameter measures the area in which the carrier density exceeds the threshold for SPP activation. In our experiment, the condition for SPP activation is fulfilled intrinsically since Re[ε] < -1. The spot size as shown in Fig. 2 cannot explain the increase in LIPSS regularity seen for distances greater than $z\text{-}z_0 = z_{Rx}$. However, the SPP active area may vary from the spot size, in particular for such distances, and therefore should be taken into consideration.

Despite finding a minimum value for DLOA in the beam focus, we see that this value is limited (~8° in stainless steel in our experiments), unlike the curvature of the wavefront which is also minimum in the focus but with a theoretical value of $|R_x|^{-1} = 0$ mm^{-1}. Although irregularities in the wavefront can reduce LIPSS regularity [25], we believe that the main limiting factor in the minimum achievable DLOA is the mean free path of SPPs, meaning that it should be characteristic of the material [21].

Therefore, our findings add another parameter to consider in the fabrication of LIPSS, in addition to the already well-known influence of laser wavelength, fluence or number of pulses [2]. Laser wavefront and, in particular, its curvature along the propagation of a laser beam, is a key aspect in the fabrication of LIPSS with high regularity. The implications of this are that special care should be put in positioning the sample in the focus of the laser beam if high spatial coherent is the desired result. Other experimental procedures currently used in LIPSS techniques, such as changing the position of the sample along the propagation axis in order to change the irradiation spot size, will also lead to LIPSS with varying regularity.

4. Conclusions

In this work, we have experimentally demonstrated the correlation between the regularity (coherence) of LIPSS and the wavefront curvature of the incident elliptical Gaussian beam. The reported results show that LIPSS with low DLOA can be found both around the beam focus and far from the focus, with a maximum DLOA in between at about the Rayleigh length from the focus. This is the same behavior exhibited by the beam waveform curvature, suggesting a strong influence in the formation of LIPSS. We explain this correlation as the result of irregularities in the excitation of SPPs and interferences that generate the LIPSS, although numerical simulations with these conditions should be performed for a better understanding of the process.

Our results imply that optimal fabrication conditions for the production of highly regular LIPSS require a good positioning of the sample in the beam propagation axis. Additionally, a highly coherent and regular wavefront is expected to help improve LIPSS regularity.

Furthermore, the presented technique is easy to implement in high-speed processing of LIPSS. This is the case in this setup, based on cylindrical focusing, where LIPSS with varying regularity are generated within a single beam pass 6 mm wide at speeds in the order of 2 mm/s resulting in a production rate of 12 mm^2/s, much higher than that obtained with spherical focusing and similar to galvanometric scanning. This value is easily scalable with laser pulse energy or repetition rate, with the advantage over other scanning techniques using small beam sizes that LIPSS regularity is uninterrupted throughout the projected line length.

We believe that the results reported in this work can contribute to advances in dynamic fabrication of LIPSS and, combined with last generation femtosecond lasers, constitute a future viable technique for LIPSS in industrial applications.

Declaration of Competing Interest

The authors declare that they have no known competing financial interests or personal relationships that could have appeared to influence the work reported in this paper.

The authors declare the following financial interests/personal relationships which may be considered as potential competing interests:

Acknowledgments

LASER4SURF has received funding from the European Union's Horizon 2020 research and innovation programme under grant agreement No 768636.

Ministerio de Economía y Competitividad (MINECO) "Ecograb" of "Programa Estatal de Investigacion, Desarrollo e Innovacion Orientada a los Retos de la Sociedad" (RTC-2016-5277-5); co-financed with structural funds of the European Union.

References

[1] T.Y. Hwang, H. Shin, H.J. Lee, H.S. Lee, C. Guo, B. Lee, Rotationally symmetric colorization of metal surfaces through omnidirectional femtosecond laser-induced periodic surface structures, Opt. Lett. 45 (2020) 3414–3417, https://doi.org/10.1364/OL.396375.

[2] J. Bonse, S. Hohm, S.V. Kirner, A. Rosenfeld, J. Kruger, Laser-induced periodic surface structures-a scientific evergreen, IEEE J. Sel. Top. Quantum Electron. 23 (2017), 9000615, https://doi.org/10.1109/JSTQE.2016.2614183.

[3] S. Gräf, F.A. Müller, Polarisation-dependent generation of fs-laser induced periodic surface structures, Appl. Surf. Sci. 331 (2015) 150–155, https://doi.org/10.1016/j.apsusc.2015.01.056.

[4] M. Martínez-Calderon, J.J. Azkona, N. Casquero, A. Rodríguez, M. Domke, M. Gómez-Aranzadi, S.M. Olaizola, E. Granados, Tailoring diamond's optical properties via direct femtosecond laser nanostructuring, Sci. Rep. 8 (2018) 14262, https://doi.org/10.1038/s41598-018-32520-0.

[5] C. Florian, J.L. Déziel, S.V. Kirner, J. Siegel, J. Bonse, The role of the laser-induced oxide layer in the formation of laser-induced periodic surface structures, Nanomaterials 10 (2020) 147, https://doi.org/10.3390/nano10010147.

[6] J. Bonse, S. Gräf, Maxwell meets marangoni—a review of theories on laser-induced periodic surface structures, Laser Photonics Rev. 14 (2020), 2000215, https://doi.org/10.1002/lpor.202000215.

[7] J.E. Sipe, J.F. Young, J.S. Preston, H.M. van Driel, Laser-induced periodic surface structure. I. Theory, Phys. Rev. B. 27 (1983) 1141–1154.

[8] A.V. Dostovalov, T.J.Y. Derrien, S.A. Lizunov, F. Přeučil, K.A. Okotrub, T. Mocek, V.P. Korolkov, S.A. Babin, N.M. Bulgakova, LIPSS on thin metallic films: New insights from multiplicity of laser-excited electromagnetic modes and efficiency of metal oxidation, Appl. Surf. Sci. 491 (2019) 650–658, https://doi.org/10.1016/j.apsusc.2019.05.171.

[9] A. Rudenko, C. Mauclair, F. Garrelie, R. Stoian, J.-P. Colombier, Amplification and regulation of periodic nanostructures in multipulse ultrashort laser-induced surface evolution by electromagnetic-hydrodynamic simulations, Phys. Rev. B. 99 (2019), 235412, https://doi.org/10.1103/PhysRevB.99.235412.

[10] R. Drevinskas, P.G. Kazansky, High-performance geometric phase elements in silica glass, APL Photonics 2 (2017) 66104, https://doi.org/10.1063/1.4984066.

[11] L. Parellada-Monreal, I. Castro-Hurtado, M. Martínez-Calderón, L. Presmanes, G. G. Mandayo, Laser-induced periodic surface structures on ZnO thin film for high response NO2 detection, Appl. Surf. Sci. 476 (2019) 569–575, https://doi.org/10.1016/j.apsusc.2019.01.115.

[12] K.M. Tanvir Ahmmed, A.-M. Kietzig, Drag reduction on laser-patterned hierarchical superhydrophobic surfaces, Soft Matter 12 (2016) 4912–4922, https://doi.org/10.1039/c6sm00436a.

[13] M. Martínez-Calderon, R.J. Martín-Palma, A. Rodríguez, M. Gómez-Aranzadi, J. P. García-Ruiz, S.M. Olaizola, M. Manso-Silván, Biomimetic hierarchical micro/nano texturing of TiAlV alloys by femtosecond laser processing for the control of cell adhesion and migration, Phys. Rev. Mater. 4 (2020) 56008, https://doi.org/10.1103/PhysRevMaterials.4.056008.

[14] M. Soldera, F. Fortuna, S. Teutoburg-Weiss, S. Milles, K. Taretto, A.F. Lasag, Comparison of structural colors achieved by laser-induced periodic surface structures and direct laser interference patterning, J. Laser Micro Nanoeng. 15 (2020) 97–103, https://doi.org/10.2961/jlmn.2020.02.2004.

[15] A. Ruiz de la Cruz, R. Lahoz, J. Siegel, G.F. de la Fuente, J. Solis, High speed inscription of uniform, large-area laser-induced periodic surface structures in Cr films using a high repetition rate fs laser, Opt. Lett. 39 (2014) 2491, https://doi.org/10.1364/ol.39.002491.

[16] L. Wang, Q.-D. Chen, X.-W. Cao, R. Buividas, X. Wang, S. Juodkazis, H.-B. Sun, Plasmonic nano-printing: large-area nanoscale energy deposition for efficient surface texturing, Light Sci. Appl. 6 (2017) e17112, https://doi.org/10.1038/lsa.2017.112.

[17] M.S. Sidhu, P. Munjal, K.P. Singh, High-fidelity large area nano-patterning of silicon with femtosecond light sheet, Appl. Phys. A Mater. Sci. Process. 124 (2018) 46, https://doi.org/10.1007/s00339-017-1459-3.

[18] S.K. Das, K. Dasari, A. Rosenfeld, R. Grunwald, Extended-area nanostructuring of TiO2 with femtosecond laser pulses at 400nm using a line focus, Nanotechnology 21 (2010), 155302, https://doi.org/10.1088/0957-4484/21/15/155302.

[19] A. San-Blas, M. Martinez-Calderon, J. Buencuerpo, L.M. Sanchez-Brea, J. del Hoyo, M. Gómez-Aranzadi, A. Rodríguez, S.M. Olaizola, Femtosecond laser fabrication of LIPSS-based waveplates on metallic surfaces, Appl. Surf. Sci. 520 (2020), 146328, https://doi.org/10.1016/j.apsusc.2020.146328.

[20] E. Granados, M. Martinez-Calderon, M. Gomez, A. Rodriguez, S.M. Olaizola, Photonic structures in diamond based on femtosecond UV laser induced periodic surface structuring (LIPSS), Opt. Express. 25 (2017) 15330, https://doi.org/10.1364/oe.25.015330.

[21] I. Gnilitskyi, T.J.Y. Derrien, Y. Levy, N.M. Bulgakova, T. Mocek, L. Orazi, High-speed manufacturing of highly regular femtosecond laser-induced periodic surface structures: Physical origin of regularity, Sci. Rep. 7 (2017) 8485, https://doi.org/10.1038/s41598-017-08788-z.

[22] A. Yariv, P. Yeh, Photonics: Optical Electronics in Modern Communications, 6th ed., Oxford University Press, 2006.

[23] J. Bonse, J. Krüger, Pulse number dependence of laser-induced periodic surface structures for femtosecond laser irradiation of silicon, J. Appl. Phys. 108 (2010), 034903, https://doi.org/10.1063/1.3456501.

[24] L. Orazi, M. Sorgato, L. Piccolo, D. Masato, G. Lucchetta, Generation and characterization of laser induced periodic surface structures on plastic injection molds, Lasers Manuf. Mater. Process. 7 (2020) 207–221, https://doi.org/10.1007/s40516-020-00115-1.

[25] H. Zhang, J.P. Colombier, C. Li, N. Faure, G. Cheng, R. Stoian, Coherence in ultrafast laser-induced periodic surface structures, Phys. Rev. B - Condens. Matter Mater. Phys. 92 (2015), 174109, https://doi.org/10.1103/PhysRevB.92.174109.

[26] A. Rudenko, C. Mauclair, F. Garrelie, R. Stoian, J.P. Colombier, Self-organization of surfaces on the nanoscale by topography-mediated selection of quasi-cylindrical and plasmonic waves, Nanophotonics 8 (2019) 459–465, https://doi.org/10.1515/nanoph-2018-0206.

[27] T.J.-Y. Derrien, J. Krüger, T.E. Itina, S. Höhm, A. Rosenfeld, J. Bonse, Rippled area formed by surface plasmon polaritons upon femtosecond laser double-pulse irradiation of silicon, Opt. Express. 21 (2013) 29643, https://doi.org/10.1364/oe.21.029643.